A PRACTICAL MODEL FOR THE HIGH-ALTITUDE RELIGHT OF A GAS TURBINE COMBUSTOR

A. Neophytou*,[1], E. Mastorakos*, E.S. Richardson, S. Stow*** and M. Zedda*****

em257@eng.cam.ac.uk

* University of Cambridge, Trumpington Street, Cambridge CB2 1PZ, UK

**Faculty of Engineering and the Environment, University of Southampton, SO17 1BG, UK

***Rolls-Royce, Derby, UK

1: Now at CERFACS, Toulouse, France

Abstract

A model that simulates the possible flame trajectories following spark ignition in a generic recirculating flame has been applied to a realistic aero-engine combustor. The model has been previously validated for gaseous and simple spray flames. It uses a CFD solution of the un-ignited flow and estimates the volume of the combustor that could be ignited given a particular flow field, spray distribution, and spark location, shape and size, and also provides a measure of the variability between independent sparking events. From this information, the ease of igniting the combustor can be assessed, and hence the combustor and injector geometry and spark placement decisions can be informed at a very early stage of the design process. Results for igniting a Rolls-Royce test combustor run with kerosene at high-altitude relight conditions for which experimental data are available and for which a RANS CFD solution has been developed, demonstrate the usefulness of the model's output. The results are consistent with experiment and also reveal that the spark characteristics and location used in the experiments, developed over a number of years by trial-and-error methods, are indeed close to optimum.

1. Introduction

Aircraft engines must satisfy high-altitude relight capability. Inexpensive models that estimate the flame propagation following spark ignition are valuable in assisting engineers during the design of combustors. Recently, various fundamental aspects of spark ignition of non-premixed systems have been revealed by experiment and simulation (for both laminar and turbulent flames) and some of the findings are reviewed in Ref. [1] and, for sprays in particular, in Ref. [2]. A physics-based model with low computational cost was presented in Ref. [3] that aimed at estimating the growth of a flame following ignition in recirculating flows by interrogating a cold CFD solution. The dominant physics found by recent experiments with recirculating flows [2, 4-6] were implemented in the model. The model reproduced the turbulent diffusion and the mean convection of the flame, the flammability limits in sprays, and the local extinction due to the turbulent stretch rate. In addition, the randomness of the turbulent transport of flame elements and the randomness of the local mixture fraction was incorporated. This led to different realisations of the flame growth with the same initial conditions of spark, as demonstrated in experiments [2, 4]. In Ref. [3], the ignition progress factor π_{ign}, defined as the volume of flammable mixture that has been ignited, was shown to be an interesting quantity to study and led to a calculation of the ignition probability (i.e. the probability that the whole flame will be ignited from depositing a spark at a given location), which agreed reasonably well with experimentally-determined distributions. The model therefore is in a state to be used in realistic geometries and sparks.

In this paper, this model is applied to a realistic kerosene combustor from Rolls-Royce [5]. Previous experimental investigations with ignition of generic recirculating spray flames showed that ignition was successful if the flame kernel was convected towards the fuel injector by the flow [2, 4-7]. In addition, a focused parametric investigation of the spark position along the side wall of the burner in Ref. [2] reached the important conclusion that the best axial location for ignition was at the maximum width of the central recirculation zone. Experiments done with the particular combustor investigated here showed that ignition has a probabilistic nature, that the time from ignition to overall flame stabilisation is between 30 ms and 50 ms, and that successful ignition is associated with a kernel that moved upstream [5]. The two last findings were also reported in a LES simulation of this combustor, presented in Ref. [8]. The flow patterns from this simulation are analyzed in the present ignition model, which intends to reproduce these findings. The statistics of π_{ign} are investigated for different spark configurations, and the location and shape of the spark, for the same spark energy, that lead to the best ignition behaviour are explored.

Firstly, we introduce the mathematical model and the combustor investigated. Then we present the results computed with the model. The paper concludes on the potential of the model in assisting the design of combustion chambers.

2. Numerical Formulation

The model was described in detail in Ref. [3], where a detailed comparison with experimental data on spark ignition with gaseous and spray flames in simple geometries is given. In this section, the main concepts of the model are repeated for clarity and the CFD solution of the gas turbine combustor is briefly presented.

2.1 Model description: main idea

The model aims at representing the possible trajectories of individual flame elements originating from a spark in a generic flow field carrying droplets. A time-averaged CFD solution of the cold flow is needed as an input to the model. The present model is based on the following steps:

1. The flow is filled with regular “grid cells” with an arbitrary size. These grid cells can have two states, cold or burnt. Initially, all grid cells are in the cold state. Cells are placed throughout the combustor volume.
2. The simulation is initialised by defining a spark volume in the domain. All grid cells that overlap with the spark volume are switched to the burnt state and each of them releases a “flame particle”. Any shape of spark can be used.
3. A flame particle is tracked with a Langevin model using the cold CFD field. A particle can extinguish according to a criterion based on a Karlovitz number, presented below. When a particle extinguishes, it is no longer computed.
4. Every time a particle visits a grid cell in a cold state, the grid cell switches to the burnt state, if the Karlovitz number permits it, and a new particle is emitted at its center and follows its own random walk.
5. Throughout the simulation, the number of cells in a burnt state divided by the total number of cells is computed as a function of time. This ratio is named “ignition progress factor” and is given the symbol π_{ign}.
6. The computation is repeated many times with different realisations. The statistics of π_{ign} for this spark location can be analysed to assess ignition performance.

By repeating this procedure for different spark locations, spark shapes etc, and comparing the resulting statistics of π_{ign} (for example, its mean and rms), the relative performance of the various sparks and of their placement can be assessed. “Good” ignition implies high values of π_{ign} at the end of the simulation, while “bad” ignition implies a low value, since the flame

would not have travelled much before it is either extinguished or convected out of the combustor. Very repeatable behaviour implies that every realisation gives similarly "good" or "bad" ignition characteristics, i.e. low variability in the final π_{ign}, which gives low rms in the statistics. In contrast, a spark or a particular spark location giving very variable ignition behaviour would be characterised by high rms of π_{ign}. The usefulness of the resulting values of π_{ign} lies more in relative comparisons, than in absolute values. The gas turbine combustor designer must strive to achieve high average and low rms of π_{ign} either by selecting the spark location and characteristics given a flow field, or by altering the flow pattern given a spark.

2.2 Mathematical formulation

The flame particle coordinate in direction i evolves according to the stochastic differential equation:

$$dX_{p,i} = U_{p,i}dt \tag{1}$$

where $U_{p,i}$ is the particle velocity in direction i. $U_{p,i}$ follows a simplified Langevin model [9] and consists of a linear drift towards the local Favre averaged velocity of the flow and an added isotropic diffusion term:

$$dU_{p,i} = -(\frac{1}{2}+\frac{3}{4}C_0)\omega_p(U_{p,i}-\tilde{U}_i)dt + (C_0\varepsilon_p dt)^{1/2}N_{p,i} \tag{2}$$

where $\tilde{U}_i$ is the local Favre averaged velocity in direction i, $N_{p,i}$ is a normally distributed variable (with mean zero and variance unity), C_0 is a constant assumed equal to 2.0 [9], ε_p is the turbulent dissipation at the particle location and ω_p is the inverse turbulent timescale at the particle location $\omega_p = u'_p/L_{turb,p}$, $u'_p = (2/3k_p)^{1/2}$ with k_p the local turbulent kinetic energy and $\varepsilon_p = k_p\omega_p$. The random variable $N_{p,i}$ for one particle is independent from another (the velocity correlation between particles is ignored). Hence, particles are simply convected by the turbulent flow and undergo random walk to model their dispersion. Equations (1) and (2) are the standard formulations of simulating turbulent dispersion in a Lagrangian framework. The initial velocity of each particle is a random Gaussian variable with a mean equal to the local Favre mean and an rms equal to the local turbulent intensity. Different realisations are obtained by setting different random distributions.

At the end of each time step dt, a criterion based on a Karlovitz number is used to assess if the flame particle extinguishes. A Karlovitz number Ka_p is defined for each particle and is compared to a critical value Ka_{crit}. If $Ka_p > Ka_{crit}$, the particle extinguishes. Ka_p is defined as the ratio between the chemical time and the reciprocal eddy lifetime [10]:

$$Ka_p = 0.157\left(\nu\frac{(u'_p)^3}{L_{turb,p}}\right)^{1/2}\frac{1}{S_{L,p}^2} \tag{3}$$

where ν is the mixture kinematic viscosity of air at the conditions studied and $S_{L,p}$ is the laminar flame speed, detailed below. The critical value Ka_{crit} was found by Abdel-Gayed and Bradley to be 1.5 for premixed flows [10], and the same critical value is used here in view of the lack of corresponding data for the extinction of turbulent spray flames.

Each particle begins its random walk from a mixture fraction sampled from a $\beta-$function pdf based on the mean and the rms of the mixture fraction from the CFD solution. The stochastic differential equation for the mixture fraction of a particle assuming interaction by exchange with the mean [9], and applying the mean evaporation rate from the local CFD cell, is given by:

$$d\xi_p = -\frac{1}{2}C_\xi \omega(\xi_p - \tilde{\xi})dt + (1-\xi_p)\frac{\overline{\Gamma}_m}{\overline{\rho}}dt \quad (4)$$

where $\overline{\rho}$ is the mean local density while Γ_m is the mass source term due to evaporation, ξ_p is the particle mixture fraction and $\tilde{\xi}$ is the local Favre averaged mixture fraction in the flow. C_ξ is a constant taken equal to 2.0 [9]. Knowledge of ξ_p enables the calculation of $S_{L,p}$ and in turn of Ka_p. The computation of the laminar flame speed as a function of the local mixture fraction $S_{L,p}$ for a gas flame is trivial, while $S_{L,p}$ in a spray is more complicated and the method used is presented in Section 2.3. As discussed in Ref. [3], validation of the present model against experiments [2,4] shows that it is valid only for high values of u'/S_L, where turbulent dispersion dominates, which is obviously the case in gas turbine combustors.

2.3 Laminar flame speed for kerosene sprays

The value of S_L, needed for the evaluation of the local Karlovitz number of the particle, must be given for sprays as a function of overall equivalence ratio ϕ_0 (i.e. using both the gaseous fuel vapour and the liquid fuel), the vapour fraction Ω, and the droplet diameter a_d. Such information can be provided experimentally or numerically. For the case of altitude relight, we need S_L at low pressure and low temperature conditions. Laminar premixed spray flame calculations with detailed chemistry that can provide the S_L needed have been performed already [11]. The results of Ref. [11] are correlated here by:

$$S_L = S_{L,max}\frac{2.5}{\sqrt{2\pi}}\exp\left(-\frac{(\phi_0-\mu)^2}{2\sigma^2}\right) \quad (5)$$

The flame speed is determined by the three parameters $S_{L,max}$, μ and σ. $S_{L,0}$ is the gaseous laminar flame speed at stoichiometry, $\mu_g = 1.07$ and $\sigma_g = 0.33$. If $\phi_0 \le 0.5$, the flame speed is set to zero; this represents the lean flammability limit. For very small droplets ($a_d \le 5\mu m$), the simulations of Ref. [11] show that the spray flame speed is virtually identical to the gaseous one, $S_{L,max} = S_{Lg,max}$, $\mu = \mu_g$ and $\sigma = \sigma_g$. For pure gas, $S_{Lg,max} = 1.01S_{L,0}$.

For larger droplets ($a_d > 5\mu m$), we use the following expressions. For n-decane at atmospheric conditions:

$$S_{L,max}(\Omega=0)/S_{L,0} = -0.0090(\ln(a_d))^3 - 0.430(\ln(a_d))^2 - 6.287(\ln(a_d)) - 28.051 \quad (6)$$

$$\mu(\Omega=0) = -0.642(\ln(a_d))^3 - 20.231(\ln(a_d))^2 - 208.844(\ln(a_d)) - 702.263 \quad (7)$$

$$\sigma(\Omega=0) = -0.412(\ln(a_d))^3 - 12.994(\ln(a_d))^2 - 134.428(\ln(a_d)) - 453.188 \quad (8)$$

For n-decane at high altitude relight conditions (P_0 =41.37 kPa, T_0 =265 K):

$$S_{L,max}(\Omega=0)/S_{L,0} = -0.0224(\ln(a_d))^3 - 0.859(\ln(a_d))^2 - 10.840(\ln(a_d)) - 44.035 \quad (9)$$

$$\mu(\Omega=0) = -0.974(\ln(a_d))^3 - 30.892(\ln(a_d))^2 - 322.963(\ln(a_d)) + 1109.328 \quad (10)$$

$$\sigma(\Omega=0) = -0.566(\ln(a_d))^3 - 17.765(\ln(a_d))^2 - 183.279(\ln(a_d)) - 619.262 \quad (11)$$

The coefficients vary linearly between $\Omega = 0$ and $\Omega = 1$ (pure gas):

$$S_{L,max} = (S_{Lg,max} - S_{L,max}(\Omega=0))\Omega + S_{L,max}(\Omega=0) \quad (12)$$

$$\mu = (\mu_g - \mu(\Omega=0))\Omega + \mu(\Omega=0) \quad (13)$$

$$\sigma = (\sigma_g - \sigma(\Omega=0))\Omega + \sigma(\Omega=0) \quad (14)$$

In the above curve-fits, a_d is to be used in microns. The original data and the above curve fits are shown in Fig. 1, where it is evident that the laminar flame speed for a spray can be high even in very rich situations, which has been explained by the fact that the flame consumes only the fuel that is available in vapour form; this could be close to stoichiometry even if there is overall much more fuel in the liquid phase. Note that the data for n-decane can be used instead of kerosene, which is the fuel of relevance to aviation gas turbines, because the two fuels have reasonably similar flame speeds [12]. Note also that the laminar flame simulations [11] show very small changes in the flame speed between atmospheric and the used relight conditions, possibly due to the detrimental effect of the low temperature being balanced by the beneficial effect of the low pressure. Therefore, to a good approximation, the data in Fig. 1 are sufficient for a range of altitudes. However it is very important to use laminar flame speed data for flames in sprays, and not in prevapourized fuels, since the SMD and ϕ_0 can affect S_L in a major way, as Fig. 1 demonstrates.

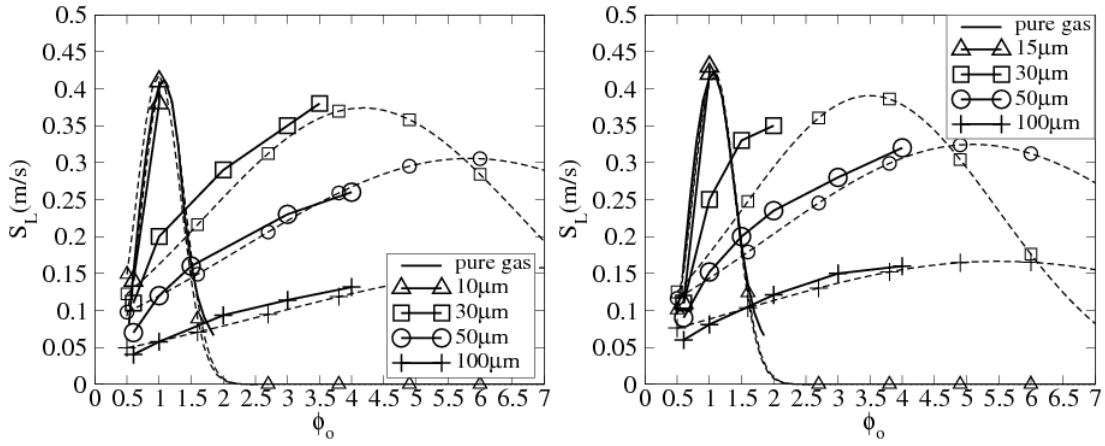

(a) (b)

Figure 1: Laminar flame speed in sprays against the overall equivalence ratio ϕ_0 for different initial droplet diameters for (a) n-decane at atmospheric conditions and (b) n-decane at high altitude ("relight") conditions (P_0=41.37 kPa, T_0=265 K). Plain lines correspond to the detailed chemistry simulation data [11], while dashed lines are computed using Eq. (5) with $\Omega = 0$.

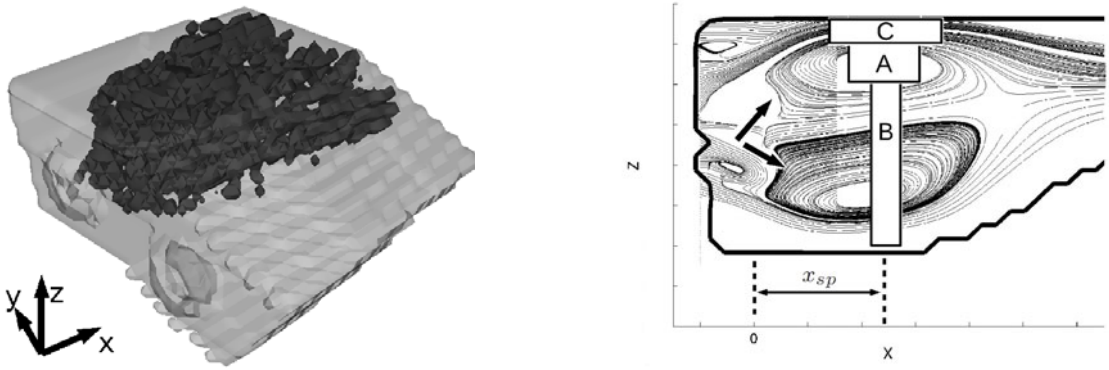

(a) (b)

Figure 2: (a) Geometry of the test combustor [5,8]. The black iso-surface shows qualitatively the fuel placement from the CFD solution of the un-ignited flow. (b) Plane $y = 0$ mm contains the axis of the cylindrical sparks studied. The two arrows show qualitatively the spray angle. The shapes of sparks A, B and C are represented.

The CFD solution (presented later) includes spray, and so the Sauter Mean Diameter (SMD), the fuel vapour mass fraction, and the fuel in liquid phase are available at every grid node, and hence S_L can be calculated. Since the turbulent kinetic energy and dissipation rate are also available from the CFD solution, the Karlovitz number of every flame particle and at every point during the particle's trajectory can be evaluated and hence the possibility of quenching is included for all times during the flame particle's evolution.

2.4 Combustor investigated and model settings

The combustion chamber is shown in Fig. 2a. The downstream direction is aligned with the x-axis. The high-altitude test rig is a two-sector rig, one sector (the left-hand sector when looking downstream) being fitted with a lean-burn injector (Rolls-Royce Deutschland Ltd & Co KG), and the other having an un-fuelled dummy injector. The fuel injected is liquid kerosene. A RANS solution of a cold flow field of this geometry was performed in the Rolls-Royce laboratories using the in-house code PRECISE (see [8] and references therein). The operating conditions chosen are given in Table 1. The RANS solution provides the three components of the mean velocity, the turbulent kinetic energy and dissipation rate, the fuel and liquid fuel mass fractions, and the Sauter Mean Diameter at every CFD grid cell. Due to the low volatility of kerosene and the cold conditions, there is virtually no fuel in vapour form in the combustor and hence $\Omega = 0$ in Eq. (12).

The flame particle tracking is performed on a rectangular Cartesian grid (which can be larger than the CFD domain). Each of these cells is initially deemed "cold". The time step in the flame particle tracking is $dt = 0.5$ ms, smaller than the estimated turbulent timescale $L_{turb}/u' = 2$ ms in the flow. The simulations stops after 60 ms, which has been found to be long enough for the flame particles to have experienced all their possible histories.

The quantity $2(C_0\varepsilon_p dt)^{1/2} dt$ is the maximum spacing for tracking the flame, as suggested in Ref. [3]. The volume-averaged turbulent dissipation rate in the domain was about 19000 $\mathrm{m}^2/\mathrm{s}^3$, the number of grid cells for the flame tracking model was 672,287, and the grid spacing was 2 mm, which satisfies this criterion. 50 independent spark events were simulated. Under those conditions, the CPU time to compute a single spark event was about 30 min in a desktop PC.

The different sparks studied are summarised in Table 2. All sparks investigated are cylindrical, the cylinder axis being aligned with the z-axis, and have the same volume (i.e. same energy). Sparks are located on the upper wall on the line $y = 0$ mm and a parametric investigation is carried out on the spark shape (length L_{sp} and diameter d_{sp} of the cylinder), and the location of the spark axis x_{sp}. The sparks studied are illustrated in Fig. 2b. The length and diameter of spark A are based on flame imaging immediately after the energy deposition [5, 6] and the cylindrical shape was chosen as representative of the penetrating sparks created by the surface discharge igniters used in gas turbines. Sparks B and C are used as a sensitivity study.

At $t = 0$, all model grid cells intersecting the spark are deemed "burnt" and a random walk of one flame particle starts from each of these burnt cells. Large sparks, therefore, emit more flame particles than small sparks. However, since the model allows for flame particle quenching if the particle is found with $Ka_p > Ka_{crit}$, it is possible that not all of these flame particles will evolve and hence the size of the spark, *per se*, does not guarantee good ignition. According to the present model, the important point is whether the spark has intersected spray with SMD and overall equivalence ratio appropriate to give a high S_L and fluid with the correct velocity. As will become evident later, this is crucial for ignition success.

Table 1: Operating conditions used in the CFD RANS simulation.

Air pressure (bar)	0.552
Air temperature (K)	278
Fuel temperature (K)	288
Normalized air mass flow	0.38
Normalized fuel-air ratio	0.56

Table 2: Different cases studied in the simulations (spark position along centerline x_{sp}, spark diameter d_{sp}, spark length L_{sp}).

Spark	x_{sp} (mm)	L_{sp} (mm)	d_{sp} (mm)
A	[0,100]	27.9	28
B	47.5	12.4	42
C	47.5	111.6	14

3. Results and Discussion

3.1 Effect of spark location

Figure 3a shows the time evolution of π_{ign} for all events for spark A at x_{sp} = 47.5 mm. In all events, π_{ign} slowly increases until $t = 10$ ms, then rapidly increases until t = 40 ms and finally stabilises to a constant value. The slow initial increase is fully consistent with experiment in both simplified [2, 4] and complex geometries [5-7]. The time duration needed to reach a stabilized value for π_{ign} provides an estimate of the time needed to ignite the whole combustor. For the present results, this time is close to the ignition timescale, about 50 ms, reported in the experiment [5] and the LES simulation of Ref. [8]. This constitutes an important validation test of the present model and suggests that the underlying physics of flame expansion for this flow is reasonably accurately included by the combination of the Langevin random walk, the generation of new flame particles from flammable regions reached by a travelling particle, and the use of a local Karlovitz number criterion.

The simulations also reproduce the stochasticity of ignition since each event results in different values of π_{ign}. Considering the values of π_{ign} for each event at the end of the simulation (t = 60 ms), a mean and a rms can be calculated, see Fig. 3a. These two quantities reveal the mean amount of burned material and the variability of ignition associated with the particular spark center and the spark shape. In Fig. 3a, the average and the rms of π_{ign} are respectively 0.19 and 0.006. The low value of the rms suggests that different events lead to fairly similar final values of burned volume. The pdf of the final π_{ign} compiled over the 50 realisations is shown in the inset.

Figure 3d shows the evolution of the mean and the rms of π_{ign} with x_{sp} (i.e. for different spark locations) for spark A. The final mean π_{ign} first increases with x_{sp}, stabilises to a relatively high value in the range 20 mm $< x_{sp} \leq 60$ mm, then decreases with x_{sp} and stabilises to a relatively low value in the range 80 mm $< x_{sp} \leq 100$ mm. Close to the injector, 0 mm $< x_{sp} \leq 20$ mm, the spark is located in a region upstream of the recirculation

zone, in the corner (Fig. 2b). The low value of the average of π_{ign} at $x_{sp} = 0$ mm indicates that in most cases, the flame does not spread and rapidly extinguishes. In addition, the high rms of π_{ign} shows that ignition there is very probabilistic so that in some events, a large volume is ignited while in others the kernel rapidly extinguishes. In this zone, there is virtually no fuel. However, due to the large spark size, some flammable material is ignited, albeit very little. Moreover, the mean convection there is positive while the turbulent kinetic energy and the turbulent dissipation are relatively high. Therefore, the ignited particles can either be brought downstream to ignite regions with more fuel or they can be transported upstream where there is no fuel leading to extinction. Hence, different realisations can lead to successful ignition events or to quickly quenched kernels. For $x_{sp} = 20$ mm, the average of π_{ign} becomes 0.19 while its rms decreases to 0.005 (Fig. 3d). This means that for a spark at x_{sp} =20 mm, most of the events ignite a relatively large volume of the combustor with a low variability. This is because there is a great overlap between the spark and the recirculation zone, see Fig. 2b. In the recirculation zone more fuel exists and ignited flame particles are easily captured by the recirculating flow and brought to the flammable region, as suggested by the experiments with recirculating sprays of Ref. [2].

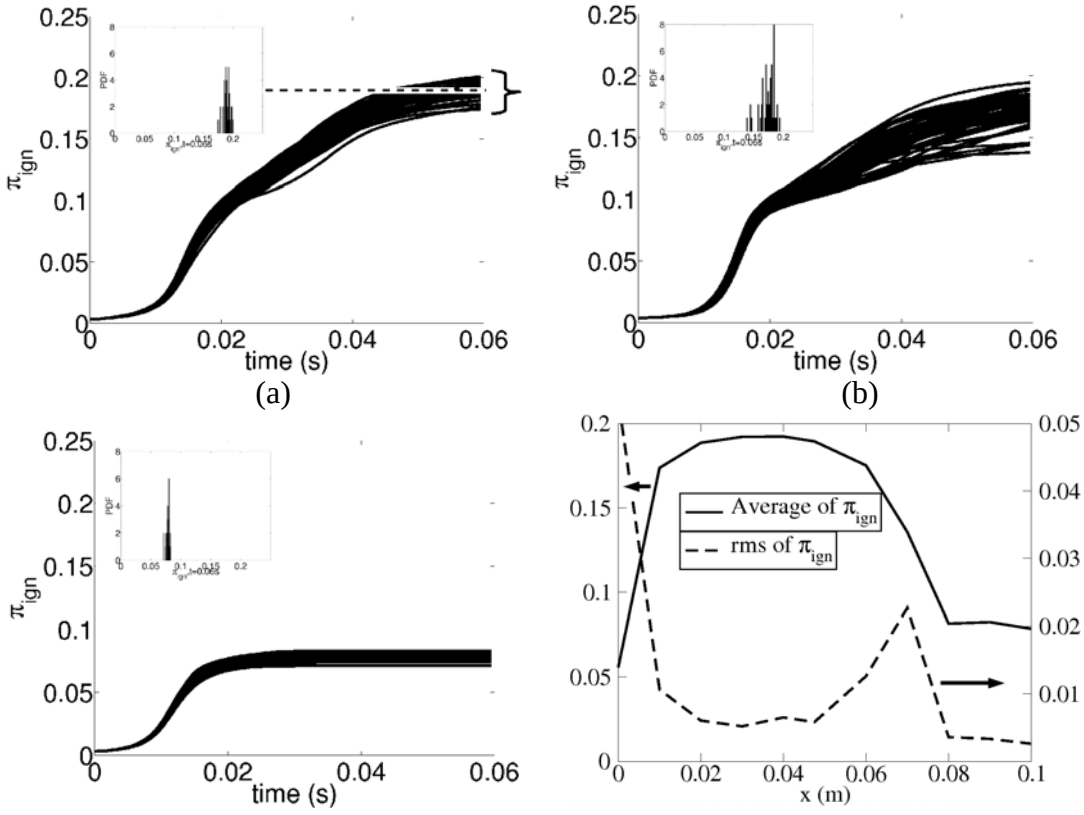

Figure 3: Time evolution of π_{ign} of individual spark events for $x_{sp} = 47.5$ mm and (a) spark A, (b) spark B and (c) spark C. The inset show the PDF of π_{ign} at the end of the simulation. (d) Average and rms of π_{ign} computed at the end of the simulation over all events *vs.* spark location along the upper wall x_{sp} for spark A.

In the region 20 mm $< x_{sp} \leq 50$ mm, Fig. 3d shows that the average and the rms of π_{ign} remain almost constant. This implies that any spark in this region will have similar ignition

performance, and that all events lead to a relatively large volume of the burner ignited. Note that this region corresponds to the maximum width of the recirculation zone. In Ref. [2], with experiments with sparks along the side wall, the best spark placement corresponded to the maximum width of the recirculation zone. Since the highest mean π_{ign} was predicted from spark locations close to where the recirculation zone is widest, the experimental recommendation has been accurately reproduced by the present model applied to realistic combustors. This provides a further validation of the usefulness of the results achieved.

Finally, in the region 50 mm $< x_{sp} \leq 80$ mm, the average of π_{ign} decreases with x_{sp} while its rms first increases with x_{sp}, reaches a peak at $x_{sp} = 70$ mm and then decreases to a relatively low value. As x_{sp} increases from 50 mm, the spark center moves further away from the maximum width of the recirculation zone and in turn the overlap between the spark and the recirculation zone is less, see Fig. 2b. Therefore, the ignited flame particles are more likely to be convected downstream by the mean flow although the random turbulent motion can occasionally bring them towards the recirculation zone. It is thus expected that the mean π_{ign} becomes lower with x_{sp}. The increase of the rms of π_{ign} is due to the increased variability. In some events all particles are convected downstream, leading to a low π_{ign} while in others turbulence moves flame particles in the recirculation zone, leading to a high π_{ign}. The location $x_{sp} = 90$ mm corresponds to the stagnation point of the recirculation zone, see Fig. 2b. Beyond this value, there is no overlap between the spark and the recirculation zone and there is little chance that the turbulent motion brings the ignited particles in the recirculation zone. The ignited flame particles are all convected downstream and never make it to the recirculation zone. Hence, they can only ignite material on their way downstream but not upstream. This leads to a low average of π_{ign} and a low rms of π_{ign} (little variability).

We conclude that the model reproduces the experimentally-observed timescale of full-flame establishment, the experimentally-determined best ignitor location, and provides useful insights concerning the stochasticity of individual ignition events. It can therefore be used by the engine designer to assist the analysis of a combustor in terms of its relight capability.

3.2 Effect of spark shape

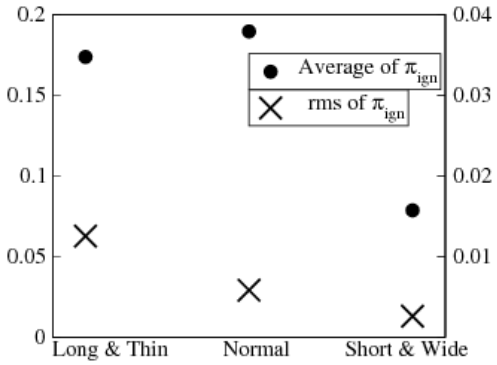

Figure 4: Average and rms of π_{ign} computed at the end of the simulation over all events with spark location $x_{sp} = 47.5$ mm for spark A (normal), B (long and thin) and C (short and wide).

In this section, the spark axis is fixed at $x_{sp} = 47.5$ mm and the statistics of π_{ign} are compared between sparks A, B and C. Note that this spark location is in the best ignition

region as shown in the previous section. Figures 3a, b and c show the evolution of π_{ign} with time for all events, respectively for spark A, B and C. Events for spark A and B both lead to relatively high values of π_{ign}. However, the variability is larger with spark B (thin and long) than with spark A. In addition, it is clear that spark C (wide and short) results in very low values of π_{ign} with all events behaving in the same way (i.e. a very narrow pdf of the final π_{ign}).

Figure 4 shows the average and the rms of π_{ign} calculated over all events at the end of the simulation for sparks A, B and C. Spark A leads to the highest value of the average of π_{ign} and a low value of the rms. Spark B has a slightly lower mean and a higher rms. Thus, events in spark A repeatedly ignite a larger volume of the combustor than sparks B and C. The behaviour of spark A is thus preferred. In the present combustor, the overall equivalence ratio is much higher on the sides of the recirculation zone than in the center (not shown here, but see Fig. 30 of Ref. [11]). Since in spark A, the spark volume is concentrated to a region of high equivalence ratio, more particles sample flammable mixtures than in spark B, where a substantial part of the spark is in the center of the recirculation zone where there is almost no fuel. The larger mass of flammable material ignited by spark A can then spread and ignite further material. This leads to higher π_{ign}. Moreover, it is possible that since spark B experiences a larger range of mean velocities and turbulence intensities than spark A, see Fig. 2b, the variability and in turn the rms of π_{ign} is higher for spark B. With spark C, the mean and the rms of π_{ign} are both low. This implies that little material is ignited in all events. This is attributed to the shape of the spark that results in little penetration in the recirculation zone, see Fig. 2b. Although the spark overlaps with flammable material, the flow tends to convect all ignited particles downstream.

The results show that a given spark energy (in the present model, spark energy is associated with the initial volume that releases flame particles; sparks A-C have the same volume) can have different ignition behaviour depending on the initial kernel's shape relative to the recirculation zone and the fuel placement. This observation is consistent with experiments [2] that showed that successful ignition from a repetitive spark in a lab-scale atmospheric spray flame happened when the turbulence happened to stretch the spark to reach inside the recirculation zone where the overall equivalence ratio was close to stoichiometric and the velocity towards the spray atomizer.

Spark A is the one used in the experiments. Its location was selected empirically in Rolls-Royce over a number of years to provide good and repeatable ignition characteristics for injectors having similar aerodynamic features to the one used here. It is interesting to note that this spark and this location was also found by the model to give the best ignition performance. This gives further credence to the techniques proposed here.

3.3 Visualization of ignition events

In this section, we show the evolution of flame particles with spark A for two different events. In the first event, $x_{sp} = 47.5$ mm and a relatively large volume of the burner is ignited. In the second event, the spark is further downstream at $x_{sp} = 100$ mm, and much less material is ignited. These two locations are representative of the best and a bad spark placement for ignition, respectively. Figures 5a and 5b shows the evolution of the computed particles for the first and the second event respectively. The green spheres denote particles that are active (i.e. have $Ka_p < Ka_{crit}$) at the instant shown, while red spheres denote particles that have already extinguished. Note that the longer the model runs the higher the

possibility that all particles will eventually extinguish, as they will eventually obtain high Ka or they will be convected out of the domain. The important output of the model is how much of the combustor has been visited by flame particles, i.e. how high π_{ign} becomes before it stabilises to a constant value.

In Fig. 5a, some particles are convected downstream just after ignition. On their path out of the combustor, they ignite many grid cells, and hence many more particles are emitted. Moreover, some particles from the spark are brought towards the recirculation zone where they ignite further grid cells. The ignition occurring in the recirculation zone contributes to a large extent to the large value of π_{ign} achieved here, see Fig. 3d. In contrast, Fig. 5b shows that in the second event, all particles are convected downstream. They ignite only grid cells on their path away from the injector, which leads to low values of π_{ign}.

Hence, these two present simulations show that π_{ign} is high when flame particles are convected upstream by the recirculating turbulent flow. This is consistent with the finding that ignition with this particular combustor was successful when the kernel moved upstream towards the fuel injector [5,6]. The particle visualizations also agree with the more general previous finding with gaseous and spray recirculating flames where ignition occurred when the spark kernel was convected by the gas towards the fuel injector [2,4].

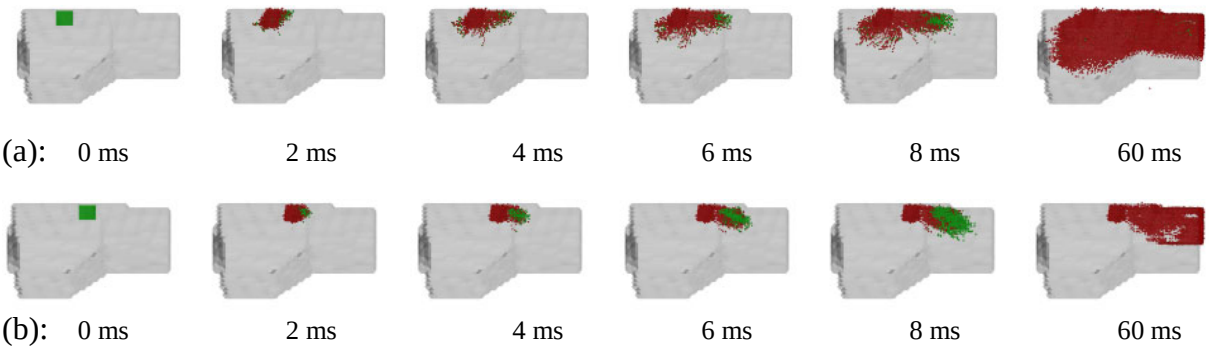

Figure 5: Evolution of particles with spark A. (a) Good ignition event (x_{sp}=47.5 mm); (b) poor ignition event (x_{sp}=100 mm). Green spheres represent particles that are still in motion (i.e. have $Ka < Ka_{crit}$). Red spheres represent extinguished particles ($Ka > Ka_{crit}$).

4. Conclusions

A model, developed to calculate the flame spread following the generation of a kernel given a cold CFD solution, has been applied to a realistic aero-engine kerosene combustion chamber. A parametric study on the characteristics and location of the cylindrical spark was performed by varying the location of the spark axis x_{sp}, the spark length L_{sp} and the spark diameter d_{sp}. For each configuration, 50 spark events were calculated and statistics on the ignition progress factor π_{ign}, i.e. the relative volume of the burner that has ignited, were compiled. The aim of the model is to enable an assessment of ignitability of different flow patterns and of various spark locations and properties without having to perform a full CFD calculation of the ignition transient.

The simulation reproduced the stochastic nature of ignition and the timescale for the flame spread, the former in qualitative and the latter in quantitative agreement with experiment with this combustor [5]. Furthermore, high values of π_{ign} were associated with

flame particles moving towards the injector, consistent with experiment [5] and previous work on recirculating gaseous and spray flames [2,4]. The region of best spark location was shown to be at the maximum width of the recirculation zone, in excellent agreement with experiments on a simplified spray burner [2]. Moreover, the optimum spark shape was suggested to be a spark volume that has a great overlap with the side of the recirculation zone, where the mixture is flammable and the recirculating flow captures the flame. It is interesting to note that the spark location that gives the best ignition performance according to the model is the one selected for injectors with similar aerodynamics after years of in-house practical experience.

Although the model has limitations and should not be considered as an exact description of the flame motion following ignition, it can be used to study qualitatively the ignition process in aero-engine combustors. Since the simulations are relatively cheap, the model can be used to carry out parametric investigations of ignition, e.g. with different spark positions, air flow rate, or fuel-air ratio, provided a reliable CFD solution of the un-ignited flow is available. Such investigations can help the designer select the spark energy, orientation and location given a particular injector early in the design process.

Acknowledgments

The work at the University of Cambridge has been funded by the Rolls-Royce Group and the European Commission through project TECC-AE (ACP7-GA-2008-211843). The work in Rolls-Royce has been funded by the European Commission through project TIMECOP-AE (AST5- CT-2006-030828). The paper reflects only the authors' views and the Community is not liable for any use that may be made of the information contained therein.

References

[1] E. Mastorakos, Prog. Energy Combust. Sci., 35:57-97, 2009.

[2] Marchione, T., Ahmed, S. F. and Mastorakos, E. *Combust. Flame*, 156:166-180, 2009.

[3] Neophytou, A. (2010) PhD Thesis, University of Cambridge. Available from http://www-diva.eng.cam.ac.uk/theses.html

[4] Ahmed, S. F. and Balachandran, R. and Marchione, T. and Mastorakos, E. *Combust. Flame*, 151:366-385, 2007.

[5] Mosbach, T. and Sadanandan, R. and Meier, W. and Eggels, R. L. G. M. Experimental Analysis of Altitude Relight Under Realistic Conditions Using Laser and High-Speed Video Techniques. In: Proc. ASME Turbo Expo 2010, Glasgow, UK, 14 - 18 June, 2010. ASME Paper GT2010-22625.

[6] Read, R. W. and Rogerson, J. W. and Hochgreb, S. Flame imaging of gas turbine relight. *AIAA Journal*, 48:1916-1927, 2010.

[7] Naegeli, D. W. and Dodge, L. G. *Combust. Sci. Technol.*, 80:165-184, 1991.

[8] Stow, S. and Zedda, M. and Triantaffylidis, A. and Garmory, A. and Mastorakos, E. and Mosbach, T. Conditional Moment Closure LES modelling of an aero-engine combustor at relight conditions. In: ASME Turbo Expo 2011, Vancouver, Canada, 6 - 10 June, 2011. Paper GT2011-45100.

[9] Pope, S. B. *Turbulent Flows*. Cambridge University Press, London, 2000.

[10] Abdel-Gayed, R. G. and Bradley, D. *Combust. Flame*, 62:61-68, 1985.

[11] Neophytou, A. and Mastorakos, E. *Combust. Flame*, 156:1627-1640, 2009.

[12] Franzelli, B. and Riber, E. and Sanjose, M. and Poinsot, T. *Combust. Flame*, 157:1364-1373, 2010.